

Unveiling causal activity of complex networks

RASHID V. WILLIAMS-GARCÍA^(a), JOHN M. BEGGS, and GERARDO ORTIZ

Department of Physics, Indiana University, Bloomington, Indiana 47405, USA

PACS 87.19.1c – Noise in the nervous system

PACS 64.60.av – Cracks, sandpiles, avalanches, and earthquakes

PACS 87.19.1j – Neuronal network dynamics

Abstract – We introduce a novel tool for analyzing complex network dynamics, allowing for cascades of causally-related events, which we call causal webs (c-webs), to be separated from other non-causally-related events. This tool shows that traditionally-conceived avalanches may contain mixtures of spatially-distinct but temporally-overlapping cascades of events, and dynamical disorder or noise. In contrast, c-webs separate these components, unveiling previously hidden features of the network and dynamics. We apply our method to mouse cortical data with resulting statistics which demonstrate for the first time that neuronal avalanches are not merely composed of causally-related events.

In systems consisting of many interacting elements, a variety of methods (*e.g.*, transfer entropy or Granger causality) are often used to reveal hidden dynamical causal links between them. This naturally leads to a complex networks description [1], raising interesting questions. For example, what fraction of the activity in such a network can be attributed to the hidden causal dynamics, and what fraction is produced by other processes, such as noise? Here we describe a new approach to this problem and demonstrate its utility on neural networks.

Over the past twenty years, there have been a number of theoretical [2–14] and experimental [15–27] attempts to connect activity in living neural networks to critical avalanches like those seen in the Bak-Tang-Wiesenfeld (BTW) sandpile model [28, 29]. It has been hypothesized that homeostatic mechanisms might *tune* the brain, a complex neural network, towards optimality associated with a critical point [30] which separates ordered (“supercritical”) and disordered (“subcritical”) phases, where cascades of activity are amplified or damped, respectively [14, 23, 26, 31, 32]. In the BTW model, grains of “sand” are dropped one at a time at random lattice locations; sites which reach a threshold height topple their grains to their neighboring sites, potentially inducing further topplings, together forming an emergent cascade of events called an avalanche. Successive topplings are thus causally related,

with each new toppling having been induced by another which happened before. The sandpile model eventually reaches a steady state in which the probability distribution of avalanche sizes follows a power law, a potential indicator of criticality. It is important to note that the grains are dropped at an infinitesimally slow rate such that the relaxation timescale, *i.e.*, the duration of the avalanches, is much shorter than the time between grain drops. This *separation of timescales* is essential to this concept of self-organized criticality (SOC) [2].

In real systems, however, this separation is not always achieved. As we will see, closer inspection of experimental neuronal avalanche data reveals potential conflicts with the SOC approach. For example, temporally distinct avalanches could be concatenated by sporadic events occurring between them, or two spatially distinct avalanches could be concatenated if they occurred synchronously. These confounding situations highlight the need for a method which clearly separates causally-related from independent activity. In our recent work, we developed a framework in which there is a **mixing of timescales**, as opposed to a separation of timescales [33]. Using this framework, it was demonstrated that access to a critical point depends on the coupling of the concerned network to an external environment, resulting in a non-zero spontaneous activation probability; the higher the probability, the further from criticality, and thus the further from optimality.

These spontaneous activation events could be caused

^(a)E-mail: rwgarcia@pitt.edu. Current affiliation: Departments of Neurobiology and Mathematics, University of Pittsburgh, Pittsburgh, Pennsylvania 15260, USA

by some unobserved influence, such as long-range innervation (in which case the network has been undersampled), or the intrinsic properties of the network elements, such as those neurons which have a propensity to fire spontaneously or are tonically active, *e.g.*, as in the case of pacemaker cells or some inhibitory neurons [34, 35]. Vanishing spontaneous activity (in combination with synaptic delays of a single time step) is effectively equivalent to a separation of timescales, as described in SOC. Thus, achieving optimality by operating at a critical point may not be feasible for a living, open neural network, according to the quasicriticality hypothesis introduced in [33], although a relative optimality may still be achieved along a nonequilibrium Widom line. The accessibility of this relatively-optimal quasicritical region will then likely depend on the character of the environment and the fundamental properties of the neural network itself. Our ability to apply the nonequilibrium Widom line framework and test the quasicriticality hypothesis, however, hinges on the ability to identify spontaneous activity in a living neural network. In this paper, we introduce a method to disentangle spontaneous neuronal activity—which we define as neuronal activations occurring without an established causal link to a prior presynaptic activation—from that which is causally-related and primarily governed by the network structure and dynamics. We focus our attention on directed networks, such as those found in living neural networks.

To this end, we next introduce the notion of **causal webs** (or c-webs for short), as a new emergent cascade of correlated events, whose properties contrast and complement those of standard avalanches. Whereas the latter are defined as spatiotemporal patterns of activation spanning a number of adjacent time steps framed by time steps lacking activity, c-webs explicitly depend on the network structure and temporal delays, thus accommodating the potential non-Markovian dynamics of complex networks. Knowledge of the network structure and delay information is key, as it allows to distinguish between different spatiotemporal patterns of activation in a way which is not possible with avalanches (see fig. 1).

Let us formalize the concept of c-webs in the context of neural networks. We label individual events by $x = (i, t)$, representing the activation of neuron i at time t , or following the notation used in [33], equivalently $z_i(t) = 1$ ($z_i(t) = 0$ meant quiescence and $z_i(t) > 1$ corresponded to refractory states, which we do not consider to be activation events). We write the set of all events $A = \{x_\mu\}$, *e.g.*, in fig. 1B, $A = \{x_1, x_2, x_3, x_4, x_5, x_6, x_7\}$. Formally, we define a c-web C as a set $C = \{p_c\}_{c=1, |C|}$ ($|C|$ being the cardinality of the set C) of correlated ordered pairs $p_c = (x_\mu, x_\nu)_c$ of events (*i.e.*, spikes), which we call **causal pairs**; quiescent and refractory neurons are not included in the set. The first and second entries, x_μ and x_ν , of the c th causal pair represent causally-related presynaptic and postsynaptic events, respectively; each activation event can be associated to at most one c-web. (Despite

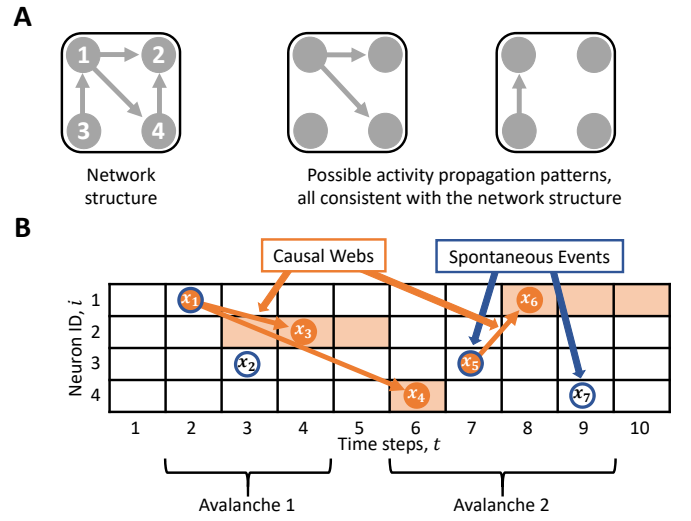


Fig. 1: (Color online) Causal webs (c-webs) are distinct from neuronal avalanches in that they rely on network structure and synaptic delays. **A.** This network produces a variety of spatiotemporal activity patterns (numbers correspond to neuron ID i). **B.** A time raster showing the activity patterns in panel **A**. Whereas only two neuronal avalanches are detected, a richer structure is revealed when spontaneous events (blue annuli) are separated from c-webs (orange disks). Acceptance windows $W_{ij}(t)$ are shaded light-orange, where i and j correspond to different neuron indices, for example, $W_{12}(2) = [3, 5]$. Notice that because of their contrasting definitions, c-webs and avalanches will generally have different statistical properties, *e.g.*, c-webs may occur over a longer span of time due to synaptic delays, as shown here.

causal relations being made in a pairwise fashion, we emphasize that this does not preclude multivariate interactions, as multiple pairings can be made to a single event.) In the following, we show how to determine those causal pairs.

A complete set of causal pairs X is constructed by taking the Cartesian product of each event x_μ with its corresponding **dynamic postsynaptic events** $\mathcal{U}(x_\mu)$, *i.e.*, $X = \bigcup_{x_\mu \in A} x_\mu \times \mathcal{U}(x_\mu)$, where $\mathcal{U}(x) \equiv \mathcal{U}(i, t)$ is the set given by

$$\mathcal{U}(i, t) = \{(j, t') \mid j \in N(i) \text{ and } t' \in W_{ij}(t)\}. \quad (1)$$

$N(i)$ refers to the set of all postsynaptic neurons j of neuron i , and $W_{ij}(t) = [t + d_{ij} - \Delta_{ij}, t + d_{ij} + \Delta_{ij}]$ is a predetermined dynamical **acceptance window**: if a postsynaptic neuron j is active within the acceptance window, then a causal link is inferred (see fig. 1B). The lower bound of the acceptance window is adjusted such that it is greater than t . We write the set of distinct events in X as $A(X) \subseteq A$.

Synaptic delays d_{ij} associated with the connection from a presynaptic neuron i to a postsynaptic neuron j , are allowed to have some uncertainty Δ_{ij} due to variability in the postsynaptic spike timing. We will later present a method by which this information can be determined from data; for the moment, we assume it is

given. In fig. 1B, synaptic delays and their uncertainties are given for the connections in fig. 1A: $d_{12} = 2$, $d_{14} = 4$, $d_{31} = 2$, and $d_{42} = 1$, with $\Delta_{12} = 1$, $\Delta_{14} = 0$, $\Delta_{31} = 1$, and $\Delta_{42} = 1$. This information can be used to determine causal pairs, *e.g.*, the event $x_1 = (1, 2)$ in fig. 1B has $\mathcal{U}(x_1) = \{x_3, x_4\}$, resulting in the causal pairs $x_1 \times \mathcal{U}(x_1) = \{(x_1, x_3), (x_1, x_4)\}$. The complete set of causal pairs for the **spacetime graph** in fig. 1B is $X = \{(x_1, x_3), (x_1, x_4), (x_5, x_6)\}$ and so $A(X) = \{x_1, x_3, x_4, x_5, x_6\}$.

A causal web represents the connected components of a directed graph whose vertices and edges are $A(X)$ and X , respectively. The example in fig. 1B thus has two c-webs, $C_1 = \{(x_1, x_3), (x_1, x_4)\}$ and $C_2 = \{(x_5, x_6)\}$. Note that spontaneous events initiate c-webs and may become part of ongoing c-webs; we call spontaneous events associated with a c-web C , its **roots** $r(C)$, *e.g.*, $r(C_1) = \{x_1\}$ and $r(C_2) = \{x_5\}$. The **size** $s(C)$ of a c-web is defined as the total number of distinct events within it. Defining that set as $A(C)$, the size $s(C)$ is then given by its cardinality: $s(C) = |A(C)|$. Note that $A(C) \subseteq A(X)$. For example, $A(C_1) = \{x_1, x_3, x_4\}$ and $A(C_2) = \{x_5, x_6\}$ in fig. 1B, with $s(C_1) = 3$ and $s(C_2) = 2$, respectively.

The **duration** $D(C)$ of a c-web C can be defined in terms of its **chord**. The chord of a c-web $K(C)$ is the sequence of distinct time steps for which there are events belonging to that c-web, arranged in ascending order in time, with no repeated elements. That is, $K(C) = (t_1, t_2, \dots, t_n)$, where t_1 and t_n are the times of the first and last events, respectively. In contrast to the definition of duration for avalanches, the length of a c-web's chord is not equal to the c-web duration. Instead, we define the duration of a c-web as a measure of its chord plus one, *i.e.*, $D(C) = 1 + \lambda(K(C))$, where $\lambda(K(C)) = t_n - t_1$. The chords of the c-webs in fig. 1B, for example, are $K(C_1) = (2, 4, 6)$ and $K(C_2) = (7, 8)$, with durations $D(C_1) = 5$ and $D(C_2) = 2$.

Finally, we define the **branching fraction** $b(C)$ of a c-web C as the average number of postsynaptic events associated with each presynaptic event:

$$b(C) = \frac{1}{s(C)} \sum_{x_\alpha \in A(C)} \sum_{c=1}^{|C|} \delta_{x_\alpha, x_\mu}, \quad (2)$$

where δ is the Kronecker delta. The first sum is evaluated over all elements x_α of $A(C)$, while the second one is over all its causal pairs $p_c = (x_\mu, x_\nu)_c$, where x_μ represents the presynaptic event of the pair $p_c \in C$. For example, in fig. 1B, $b(C_1) = 2/3$ and $b(C_2) = 1/2$.

We performed tests of our method using simulations of the cortical branching model (CBM) [33]. In the CBM, spontaneously activated nodes initiate cascades of activity which spread to neighboring nodes depending on their state (*i.e.*, quiescent, active, or refractory) and activity transmission probabilities (*i.e.*, connection weights); there are no inhibitory nodes in the simplest formulation of the CBM. As we have stated earlier, neuronal avalanches and c-webs should coincide as emergent cascades of correlated

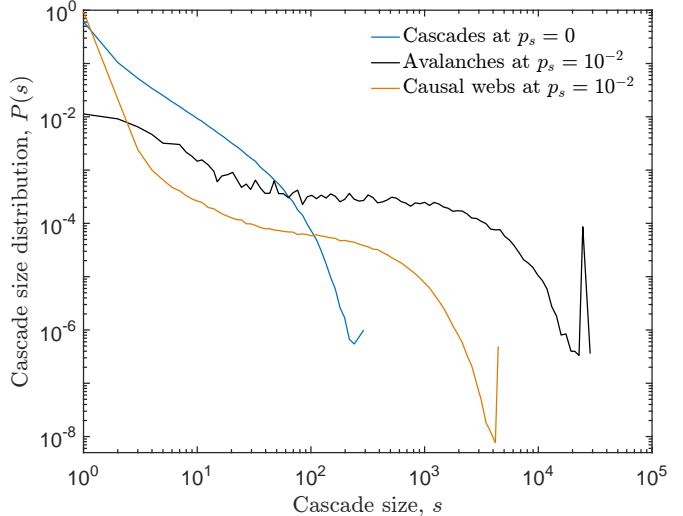


Fig. 2: (Color online) Simulated avalanche and causal web size distributions coincide in the case of a separation of timescales (blue), but are substantially different under conditions corresponding to a mixing of timescales (orange/black).

events in the limits $p_s \rightarrow 0$ for all nodes and $d_{ij} = 1$ for all pairs of nodes (i, j) . We simulated 10^6 avalanches on a network of $N = 243$ nodes, whose structure and synaptic weights were inspired by experimental data; all synaptic delays were set to a single time step, *i.e.*, $d_{ij} = 1$. To simulate the $p_s \rightarrow 0$ limit (a separation of timescales), we initiated avalanches at single, random nodes, only starting a new avalanche when the previous one had finished; no spontaneous events or concurrent avalanches were allowed. The resulting avalanche and c-web size probability distributions were identical, as expected (see fig. 2). In order to examine these distributions under conditions corresponding to a mixing of timescales, we allowed for nodes to become active spontaneously. Spontaneous activation probabilities for each node were drawn from a Gaussian distribution with mean and standard deviation of 10^{-2} ; negative values were set to zero. As a result, the two distributions differ greatly; most notably, c-webs better capture the abundance of isolated spontaneous events ($s = 1$ c-webs) than avalanches do.

In another test, we constructed a random network of $N = 360$ nodes, each with an in-degree of $k_{in} = 3$, as in [33]. The network was not strongly connected (*i.e.*, it was reducible, thus contained subgraphs) and had a spectral radius (*i.e.*, Perron-Frobenius eigenvalue) of $\kappa = 0.23$. Synaptic delays (in time steps) were drawn from a uniform distribution of integers in a closed interval, $d_{ij} \in [1, 16]$. Spontaneous activation probabilities for each node were drawn from a Gaussian distribution with mean and standard deviation of 10^{-4} ; negative values were again set to zero. The simulation was performed over 3.6×10^6 time steps and refractory periods of all nodes were set to a single time step (or, in the language of [33], $\tau_r = 1$).

Spontaneous events detected by our method were used to construct a new spontaneous activation probability distribution, which we compared with the initial distribution using a Kolmogorov-Smirnov (KS) test at a 5% significance level: the distributions were in agreement with a p-value of 0.996 [36]. We note that as the overall connectivity of the network (which we quantify by κ , as in [33]) is increased, spontaneous events become less prominent as c-webs begin to dominate the dynamics, leading to more driven activations (and, when $\tau_r > 1$, refractory nodes), thus preventing spontaneous events: neural network dynamics present a fluctuating bottleneck to the influence of an environment.

To determine the c-webs, we have so far assumed knowledge of the network structure and delay information (*i.e.*,

the d_{ij} and Δ_{ij} 's), however in practice, this information must be learned from experimental data. We now describe a method, based on delayed transfer entropy (TE) [37,38], by which this information can be established from high temporal resolution multiunit timeseries data. The use of TE is not absolutely necessary; alternative measures of effective connectivity and causal effect, such as information flow, which also compute conditional probabilities directly from data, could in principle be used [39,40]. The notion of c-webs is completely independent of any one measure of effective connectivity.

For a particular pair of neurons (i,j) , TE is calculated at various synaptic delays d , peaking at the appropriate $d = d_{ij}$, with a width of Δ_{ij} [37]. At a given d , the TE from neuron i to neuron j , is given by

$$T_{i \rightarrow j}(d) = \sum_{\mathbf{z}_{i \rightarrow j}(d)} p(z_j(t-1), z_j(t), z_i(t-d)) \log_2 \left(\frac{p(z_j(t)|z_j(t-1), z_i(t-d))}{p(z_j(t)|z_j(t-1))} \right), \quad (3)$$

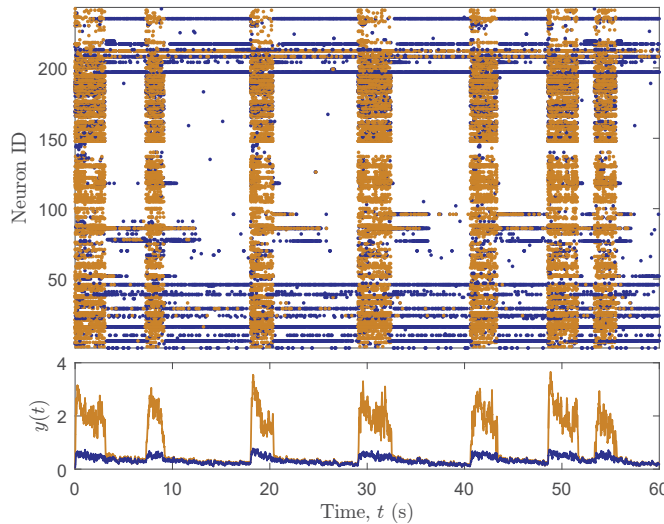


Fig. 3: (Color online) One minute of neural network activity recorded from somatosensory cortex, after processing to separate spontaneous events (dark blue) from c-webs (orange) using the c-webs method. Note that tonically-active neurons mainly produce spontaneous events.

where $\mathbf{z}_{i \rightarrow j}(d) = \{z_j(t-1), z_j(t), z_i(t-d)\}$ indicates that the sum is performed over all possible configurations of the binary variables $z_j(t-1)$, $z_j(t)$, and $z_i(t-d)$. Joint and conditional probabilities in eq. (3) are estimated from spike-sorted data, as in [37]. For every pair of neurons (i,j) , $T_{i \rightarrow j}(d)$ is computed over a range of values $d \in [1, 16]$; the peak value $T_{i \rightarrow j}(d_{ij})$ represents the putative connection from neuron i to neuron j . The spike data is then randomly shuffled to establish a rejection threshold; TE values below this threshold are not considered to

be significant and are set to zero [37, 41]. The remaining TE values are then converted to activity transmission probabilities, as described in the supplemental materials of [42], which assumes that spiking activity is Poisson-distributed. Note that the c-webs method could potentially be further improved by stochastically establishing causal pairs depending on those probabilities. Spurious connections, such as those due to common drive and transitive connections, are removed by considering synaptic delays of the significant connections; these results “were valid over a wide range of values of the rejection threshold” [43]. We use only the synaptic delays d_{ij} of the significant connections to establish causal pairs.

We next demonstrate the utility of our method when applied to experimental data (see fig. 3). For our demonstration, we have used ten data sets from [44], which were collected *in vitro* from organotypic cultures of mouse somatosensory cortex using a 512-microelectrode array with a 60 μ m electrode spacing and a 20 kHz sampling rate over hour-long recordings [45, 46]. Applying our method to a data set containing $N = 243$ neurons, spontaneous events are highlighted in dark blue and c-webs in orange to illustrate their qualitative differences; note that spontaneous events may initiate or contribute to c-webs as in fig. 1B. In fig. 3, an activity time raster (top panel) is presented along with the corresponding timeseries of the activity (bottom panel), on which we have performed a moving average with a $\Delta t = 100$ ms window: $y(t) = \sum_{t'=0}^{\Delta t-1} x(t-t')/\Delta t$, where $x(t) = \sum_{i=1}^N \delta_{z_i(t),1}$ [47].

We next performed simulations of the CBM using information extracted from the experimental data with TE and from applying the c-webs method, *i.e.*, the activity transmission probabilities (synaptic weights), synaptic delays, and spontaneous events. Using a data set which contained $N = 435$ neurons, the synaptic weights were ad-

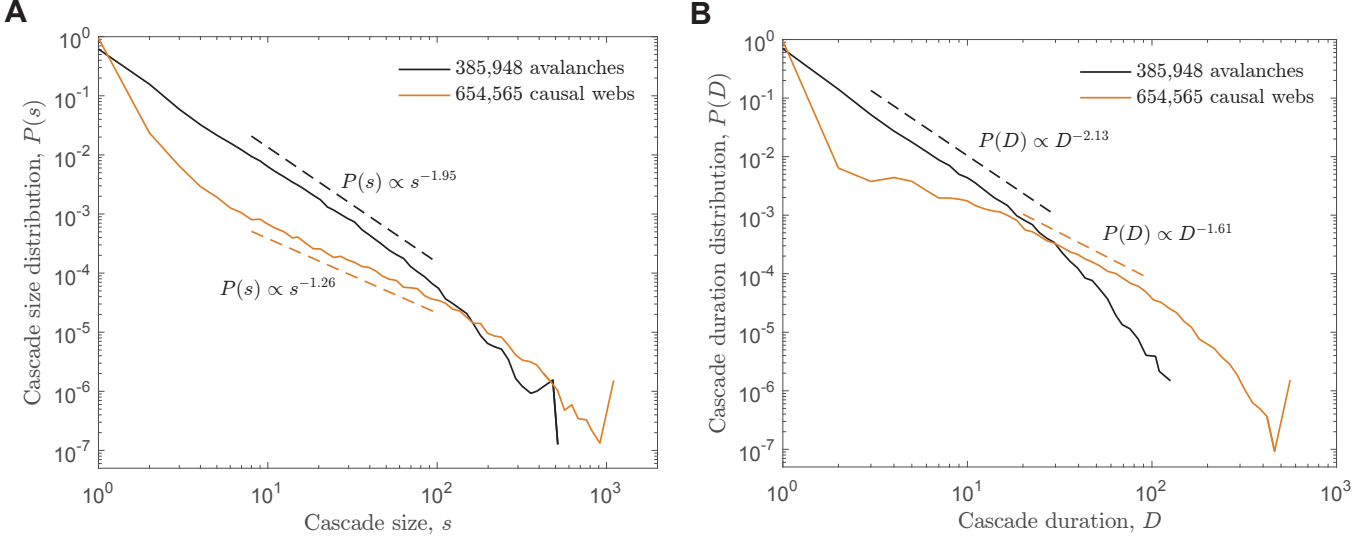


Fig. 4: (Color online) Cascade size (A) and duration (B) probability distributions from simulations, which used the network structure, synaptic delays, and times of spontaneous events extracted from *in vitro* data using TE and c-webs analyses.

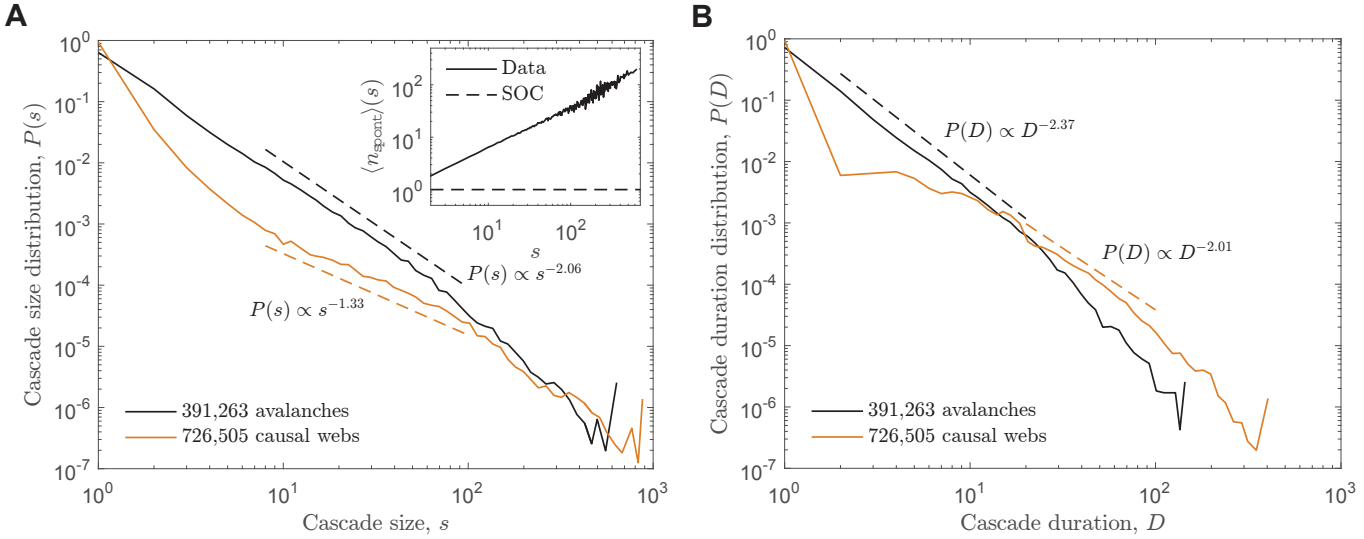


Fig. 5: (Color online) Cascade size (A) and duration (B) probability distributions from *in vitro* data. Avalanches (black) and c-webs (orange) exhibit different statistical properties and scaling due to a mixing of timescales (panel A inset). Dashed lines represent scaling regions over which maximum likelihood estimates were performed. Compare with the simulated predictions in fig. 4.

justed by a factor κ (to manipulate the Perron-Frobenius eigenvalue of the corresponding adjacency matrix) over the range $[0.20, 1.40]$ in steps of $\Delta\kappa = 0.05$ and performed simulations at each value of κ —the raw data had a Perron-Frobenius eigenvalue of $\kappa \approx 0.31$. Instead of stochastically initiating activity cascades using a fixed value of the spontaneous activation probability p_s (as in [33]), we used the spontaneous events identified from the data to initiate activity; as a result, each node exhibited a vastly different number of spontaneous activations. Refractory periods for each node were set to 1 time step and simulations were run over 3.6×10^6 time steps. The resulting avalanche

(defined in 1 ms bins) and c-web size and duration probability distributions for simulations performed at $\kappa = 0.80$ are plotted in fig. 4 using a logarithmic binning of 1.1 (for a description of log-binning, refer to Appendix E of [29]).

In fig. 5, we plot size and duration probability distributions (again with logarithmic binning of 1.1) using avalanches and c-webs identified directly from the data; as predicted in fig. 1, maximum c-web durations were longer than those of avalanches in all ten data sets. Maximum likelihood estimation of the power law exponents was performed over the scaling regions indicated by the dashed lines in fig. 5 using the methods described in [48]. This

analysis produced exponents of 2.06 and 1.33 with log-likelihoods -3.47 and -4.05 for avalanche and c-web sizes, respectively (see fig. 5A). The avalanche and c-web duration distributions (fig. 5B) featured exponents of 2.37 and 2.01 with log-likelihoods of -1.70 and -3.96 , respectively. Additionally, we note the emergence of isolated spontaneous activation events ($s = 1$ c-webs) and dominance over larger c-webs, which does not fit the traditional picture of avalanche criticality. This demonstrates that while neuronal avalanches may exhibit approximate power-law scaling, thus suggesting potential underlying critical behavior, the corresponding c-web distributions do not; this is apparent from both a qualitative and quantitative examination. Although we have not determined whether the data feature quasicritical dynamics, operating at or near the nonequilibrium Widom line, these results strongly suggest non-critical dynamics. To further illustrate how avalanches confound important dynamical information in the data, we plotted the average number of spontaneous events $\langle n_{\text{spont}} \rangle(s)$, contained in avalanches as a function of their size s , and compared this to the expected result from a situation with a separation of timescales (which we verified using simulations), where SOC would be applicable (see fig. 5A inset). In other words, our results put the application of the SOC framework to complex neural network dynamics into question.

The ability to disentangle independent cascades of activity not only allows us to apply the nonequilibrium Widom line framework and discriminate criticality from quasicriticality, but also allows us to examine the dynamics of living neural networks in novel ways. For example, it has been suggested that a reduced signal-to-noise ratio (SNR) produces inefficient hyperactivation in the pre-frontal cortices of schizophrenics during successful cognitive tasks [49]. This hypothesis has been supported by computational models showing that neural network attractors become unstable with increased noise [50]. Thus c-webs could be used to examine the neural basis of hyperfrontality for the first time. Another potential application is the identification of different classes of network nodes. For instance, because inhibitory neurons exhibit different firing patterns from excitatory neurons, namely fast-spiking and tonic activation [34, 35], and because we have found tonic activations to be mostly spontaneous (*cf.* fig. 3), distributions of spontaneous neuronal events may help identify inhibitory neurons, complementing previously-established methods [51]. This may provide further insight into the nature of rapid eye movement sleep, recently been shown to be induced by the activation of inhibitory neurons [52]. The latter may lead to a decreased SNR, as in the portions of fig. 3 dominated by spontaneous events. We note, however, that because inhibitory neurons suppress (rather than induce) activation cascades, the c-webs method alone cannot be used to definitively identify inhibitory neurons; the method cannot distinguish inhibitory activity from other kinds of activity occurring in the network. Our method may also

inform understanding of the neural network structure beyond the capabilities of currently available methods. In the case of network undersampling, hidden network cycles might be discovered by employing our approach in conjunction with population coupling methods [53]. Moreover, c-webs may enable us to distinguish recurrent from feed-forward network dynamics. Notice that the use of c-webs also obviates the need to choose a particular temporal binning, contrasting neuronal avalanches which can strongly depend on the choice of binning [16, 17, 54]. And although spurious connections detected by TE have been minimized using recent methods, other issues and limitations accompany its use, which for instance requires establishing a suitable threshold for accepting putative connections [37, 43]. These projects merit further investigation.

Similar applications could be envisioned for complex networks in general. For example, financial networks could be decomposed into agents that directly interact through exchanges as well as exogenous factors like weather or inflation. In climate research, identifying causal connections between different geographic regions is important for understanding the impact of localized events on global climate [55]. In models of disease spreading, such as the SIRS model, c-webs could differentiate between sources of infection [56]. Such an approach is likely to be useful whenever considering interacting units, whether they are people in social networks, species in ecological webs, or protein molecules in a stochastic environment. A specific application in social media could involve the detection of Twitterbots and astroturfing [57].

The authors would like to thank Hadi Hafizi, Emily B. Miller, Benjamin Nicholson, and Zachary C. Tosi for valuable discussions, as well as Shinya Ito, Alan M. Litke, and Fang-Chin Yeh for providing their *in vitro* data. R. V. Williams-García is presently supported by a National Institutes of Health Ruth L. Kirschstein National Research Service Award, T32 NS086749.

REFERENCES

- [1] GROS C., *Complex and Adaptive Dynamical Systems* (Springer-Verlag, Berlin) 2013.
- [2] BAK P., *How Nature Works: The Science of Self-Organized Criticality* (Springer-Verlag, New York) 1996.
- [3] BERTSCHINGER N. and NATSCHLAGER T., *Neural Comput.*, **16** (2004) 1413.
- [4] CHIALVO D. R., *Physica A*, **340** (2004) 756.
- [5] HALDEMAN C. and BEGGS J. M., *Phys. Rev. Lett.*, **94** (2005) 058101.
- [6] KINOUCHI O. and COPELLI M., *Nat. Phys.*, **2** (2006) 348.
- [7] LEVINA A., HERRMANN J. M., and GEISEL T., *Nat. Phys.*, **3** (2007) 857.
- [8] KITZBICHLER M. G. *et al.*, *PLoS Comput. Biol.*, **5** (2009) e1000314.
- [9] CHEN W. *et al.*, *BMC Neurosci.*, **11** (2010) 3.

[10] LARREMORE D. B. *et al.*, *Phys. Rev. Lett.*, **106** (2011) 058101.

[11] MORA T. and BIALEK W., *J. Stat. Phys.*, **144** (2011) 268.

[12] PEI S. *et al.*, *Phys. Rev. E*, **86** (2012) 021909.

[13] MANCHANDA K. *et al.*, *Phys. Rev. E*, **87** (2013) 012704.

[14] RYBARSH M. and BORNHOLDT S., *PLoS ONE*, **9** (2014) e93090.

[15] WORRELL G. A. *et al.*, *Neuroreport*, **13** (2002) 2017.

[16] BEGGS J. M. and PLENZ D., *J. Neurosci.*, **23** (2003) 11167.

[17] PASQUALE V. *et al.*, *Neuroscience*, **153** (2008) 1354.

[18] POIL S. S., VAN OOVEN A., and LINKEKAER-HANSEN K., *Hum. Brain Mapp.*, **29** (2008) 770.

[19] SHEW W. L. *et al.*, *J. Neurosci.*, **29** (2009) 15595.

[20] RIBEIRO T. L. *et al.*, *PLoS ONE*, **5** (2010) e0014129.

[21] SHEW W. L. *et al.*, *J. Neurosci.*, **31** (2011) 55.

[22] G. SOLOVEY *et al.*, *Front. Integr. Neurosci.*, **6** (2012) 44.

[23] PRIESEMANN V. *et al.*, *PLoS Comput. Biol.*, **9** (2013) e1002985.

[24] SHRIKI O. *et al.*, *J. Neurosci.*, **33** (2013) 7079.

[25] YU S. *et al.*, *Front. Sys. Neurosci.*, **2013** (7) .

[26] DE ARCANGELIS L. *et al.*, *J. Stat. Mech.*, **2014** (2014) P03026.

[27] SHEW W. L. *et al.*, *Nat. Phys.*, **11** (2015) 659.

[28] BAK P., TANG C., and WIESENFELD K., *Phys. Rev. Lett.*, **59** (1987) 381.

[29] CHRISTENSEN K. and MOLONEY N. R., *Complexity and Criticality* (Imperial College Press, London) 2005.

[30] NISHIMORI H. and ORTIZ G., *Elements of Phase Transitions and Critical Phenomena* (Oxford University Press, New York) 2011.

[31] HSU D. and BEGGS J. M., *Neurocomputing*, **69** (2006) 1134.

[32] PEARLMUTTER B. A. and HOUGHTON C. J., *Neural Comput.*, **21** (2009) 1622.

[33] WILLIAMS-GARCÍA R. V., MOORE M., BEGGS J. M., and ORTIZ G., *Phys. Rev. E*, **90** (2014) 062714.

[34] FREUND T. F. and BUZSÁKI G., *Hippocampus*, **6** (1996) 347.

[35] HU H. *et al.*, *Science*, **345** (2014) 1255263.

[36] JAMES F., *Statistical Methods in Experimental Physics* (World Scientific, Singapore) 2006.

[37] ITO S. *et al.*, *PLoS ONE*, **6** (2011) e27431.

[38] WIBRAL M. *et al.*, *PLoS ONE*, **8** (2013) e55809.

[39] AY N. and POLANI D., *Advances in Complex Systems*, **11** (2008) 17.

[40] LIZIER J. T. and PROKOPENKO M., *Eur. Phys. J. B*, **73** (2010) 605.

[41] BEGGS J. M. and PLENZ D., *J. Neurosci.*, **24** (2004) 5216.

[42] FRIEDMAN N., ITO S., BRINKMAN B. A. W., SHIMONO M., DEVILLE R. E. L., DAHMEN K. A., BEGGS J. M., and BUTLER T. C., *Phys. Rev. Lett.*, **108** (2012) 208102.

[43] NIGAM S. *et al.*, *J. Neurosci.*, **36** (2016) 670.

[44] ITO S., YEH F. C., TIMME N. M., HOTTONY P., LITKE A. M., AND BEGGS J. M. (2016), *Spontaneous spiking activity of hundreds of neurons in mouse somatosensory cortex slice cultures recorded using a dense 512 electrode array*. CRCNS.org, <http://dx.doi.org/10.6080/K07D2S2F>

[45] LITKE A. M. *et al.*, *IEEE Transactions on Nuclear Science*, **51** (2004) 1434.

[46] ITO S. *et al.*, *Plos ONE*, **9** (2014) e105324.

[47] OPPENHEIM A. V. *et al.*, *Discrete-Time Signal Processing* (Prentice Hall, Englewood Cliffs) 1989.

[48] MARSHALL N. *et al.*, *Front. Physiol.*, **7** (2016) 250.

[49] WINTERER G. and WEINBERGER D. R., *Trends Neurosci.*, **27** (2004) 683.

[50] ROLLS E. T. *et al.*, *Nature*, **9** (2008) 696.

[51] BARTHÓ P. *et al.*, *J. Neurophysiol.*, **92** (2004) 600.

[52] WEBER F. *et al.*, *Nature*, **526** (2015) 435.

[53] OKUN M. *et al.*, *Nature*, **521** (2015) 511.

[54] PLENZ D. *et al.*, *Criticality in Neural Systems* (Wiley-VCH, Weinheim) 2014.

[55] RUNGE J. *et al.*, *Nat. Commun.*, **6** (2015) 8502.

[56] ANDERSON R. M. and MAY R. M., *Nature*, **1979** (280) .

[57] RATKIEWICZ J., CONOVER M. D., MEISS M., GONÇALVES B., PATIL S., FLAMMINI A., and MENCZER F., in *Proceedings of the 20th international conference companion on world wide web* (ACM, New York) 2011, p. 249.